Journal of Geophysical Research: Atmospheres

Supporting Information for

Retrieval of Tropospheric Water Vapour from Airborne Far-infrared Measurements: A Case Study

L. Warwick[1], H. Brindley[1,2], A. Di Roma[3], S. Fox[4], S. Havemann[4], J. Murray[1], H. Oetjen[5], H. C. Price[6], D. Schuettemeyer[5], L. Sgheri[7], D. A. Tiddeman[4]

[1]Space and Atmospheric Physics, Imperial College London, UK

[2]NERC National Centre for Earth Observation, Imperial College, London, UK

[3]Istituto di Scienze dell'Atmosfera e del Clima, ISAC-CNR, Bologna, Italy

[4]Met Office, Exeter, UK

[5]ESA, ESTEC, The Netherlands

[6]FAAM Airborne Laboratory, UK

[7]IAC – CNR, Sesto Fiorentino (FI), Italy

Corresponding author: Laura Warwick (laura.warwick14@imperial.ac.uk)

Contents of this file

Introduction

This supporting material contains plots showing a-priori variance covariance matrices, averaging kernels and the standard deviation for retrievals carried out in the paper and a more detailed investigation of the apparent bias in the TAFTS measurements between 440 and 520 cm^{-1}.

Text S1.

Supplementary figure S1 shows the a-priori temperature and water vapour variance covariance matrices for all retrievals carried out in this study. Figures S2 and S3 show additional plots for the TAFTS reduced scale temperature and water vapour retrieval described in section 4.3 and the ARIES temperature and water vapour retrieval from section 5.1.

Figure S2 shows the temperature and water vapour averaging kernels for both TAFTS and ARIES plotted against height. The TAFTS water vapour averaging kernels are generally sharper than the ARIES averaging kernels indicating that the TAFTS retrieval is more sensitive to changes in the true atmospheric profile. The temperature averaging kernels for both TAFTS and ARIES are generally lower than those for water vapour.

Figure S3 shows a comparison of the standard deviation for temperature and water vapour profiles for the a-priori and TAFTS and ARIES retrievals. Below around 6 km the ARIES temperature retrieval has lower standard deviation than TAFTS. However, for water vapour, the TAFTS retrieval has a lower standard deviation throughout the profile.

Text S2.

The aim of this set of studies was to investigate potential causes for the differences of 3-5 mW m^{-2} sr^{-1} $(cm^{-1})^{-1}$ seen between the TAFTS simulations and measurements between 440 and 520 cm^{-1} highlighted in section 4.2 of the paper. The sensitivity of the simulation to changes in surface temperature, surface emissivity, water vapour foreign continuum strength and water vapour line widths were investigated.

First, the effect of surface temperature was examined. In this test 3 surface temperatures were used (280.50, 280.75, 281.00K) chosen so they would produce radiance signals falling within the ARIES measurement uncertainty range across the atmospheric window. Simulations were produced using the atmospheric profiles from the dropsonde case, with only the surface temperature altered. Figure S4 shows the differences between these simulations and the simulation produced using the estimate of surface temperature from the IREMIS model (280.25K). As expected, the differences are most noticeable in the atmospheric window, however some change in radiance is noticeable in the far-infrared between 400 and 600 cm^{-1}. However, this radiance difference caused by changing surface temperature is at most 10% of the bias in the TAFTS shortwave spectra between 350 and 600 cm^{-1}.

However, as the TAFTS shortwave measurements are clearly sensitive to surface conditions, a second test was carried out to investigate the effect of varying surface emissivity on the expected far-infrared radiance. As ocean emissivity in the far-infrared has not been experimentally determined, error in the surface emissivity used in the simulation could be a cause for some of the apparent bias in the TAFTS observations. To test this a simulation was performed using the atmosphere and surface temperature of the dropsonde simulation but with an emissivity of 1 throughout the spectrum, representing the maximum possible positive error in the emissivity. Figure S5 shows the radiance difference between this simulation and the standard dropsonde simulation. The largest difference in radiance between 440 and 520 cm^{-1} is 1.5 mW m^{-2} sr^{-1} $(cm^{-1})^{-1}$ which is not sufficient to explain the entirety of the bias in this region.

Another phenomenon which could be causing systematic bias in the simulations is a misrepresentation of the water vapour continuum (Harries et al., 2008). Recent work

suggests an uncertainty of up to 20% in the strength of the water vapour continuum at wavenumbers below 400 cm^{-1} and of 7% at wavenumbers between 400 and 600 cm^{-1} (Mlawer et al., 2019). We thus perturb the strength of the water vapour continuum in LBLRTM by ±10% and ±20% keeping all other aspects of the simulation the same as for the dropsonde simulation. Figure S6 shows the impact of these changes on the simulated spectra. The uncertainty in the continuum has the largest impact between 350 and 500 cm^{-1} with significant changes seen throughout the far-infrared. However, perturbations of this magnitude to the water vapour continuum are insufficient to explain the bias seen between 440-520 cm^{-1}.

We also investigate the impact of altering the water vapour line widths in line with the uncertainties reported in the AERv3.8 database (the H_2O line parameters in AERv3.8 are based on the HITRAN 2012 database, Rothman et al. 2013). Three simulations were performed, an unperturbed case, a case where all the water vapour line widths were reduced and a case where all water vapour line widths were increased by the quoted uncertainty. The atmospheric profiles and surface properties were the same as those used in the dropsonde simulation. Figure S7 shows the change in radiance at the measurement altitude caused by this change in spectroscopic parameters. The maximum value of this radiance change is 0.7 mW m^{-2} sr^{-1} $(cm^{-1})^{-1}$ at around 430 cm^{-1}. Although this impact is in the region where the difference is seen between measurements and simulations, the size of the difference is less than a quarter of the observed difference.

When all the perturbations in this section are summed the overall maximum difference in radiance is around 2.9 mW m^{-2} sr^{-1} $(cm^{-1})^{-1}$. This is just smaller than the minimum size of the bias between the observations and simulations.

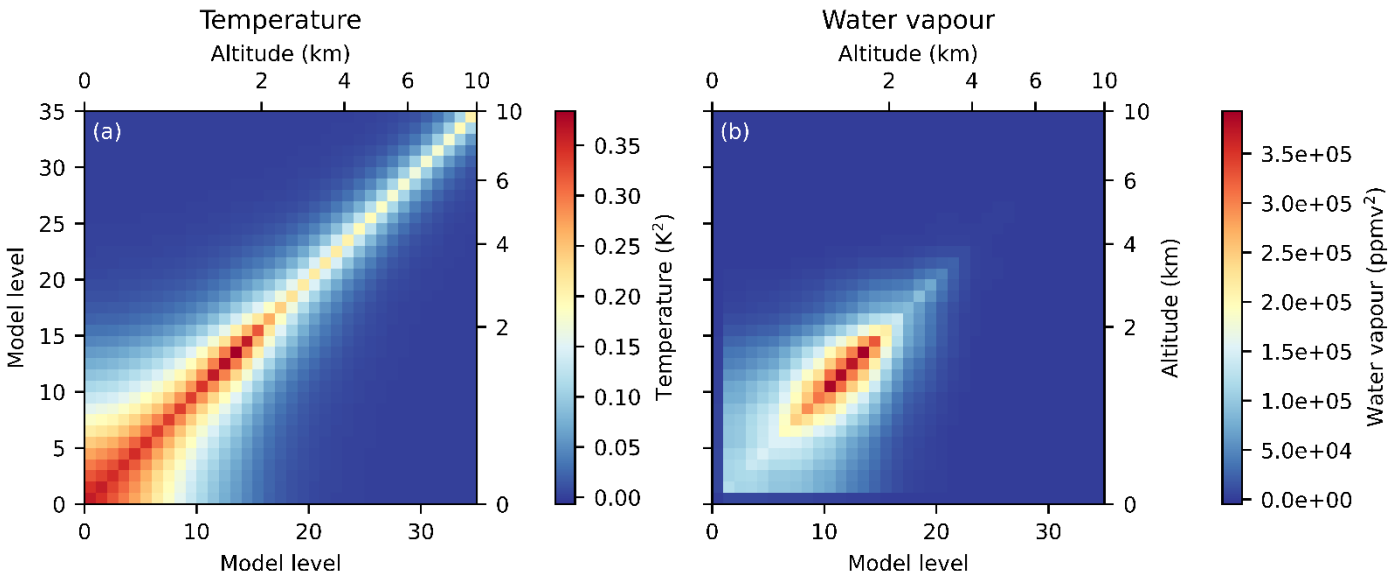

Figure S1. A-priori variance covariance matrices for (a) temperature and (b) water vapour for the retrieval tests performed throughout the paper.

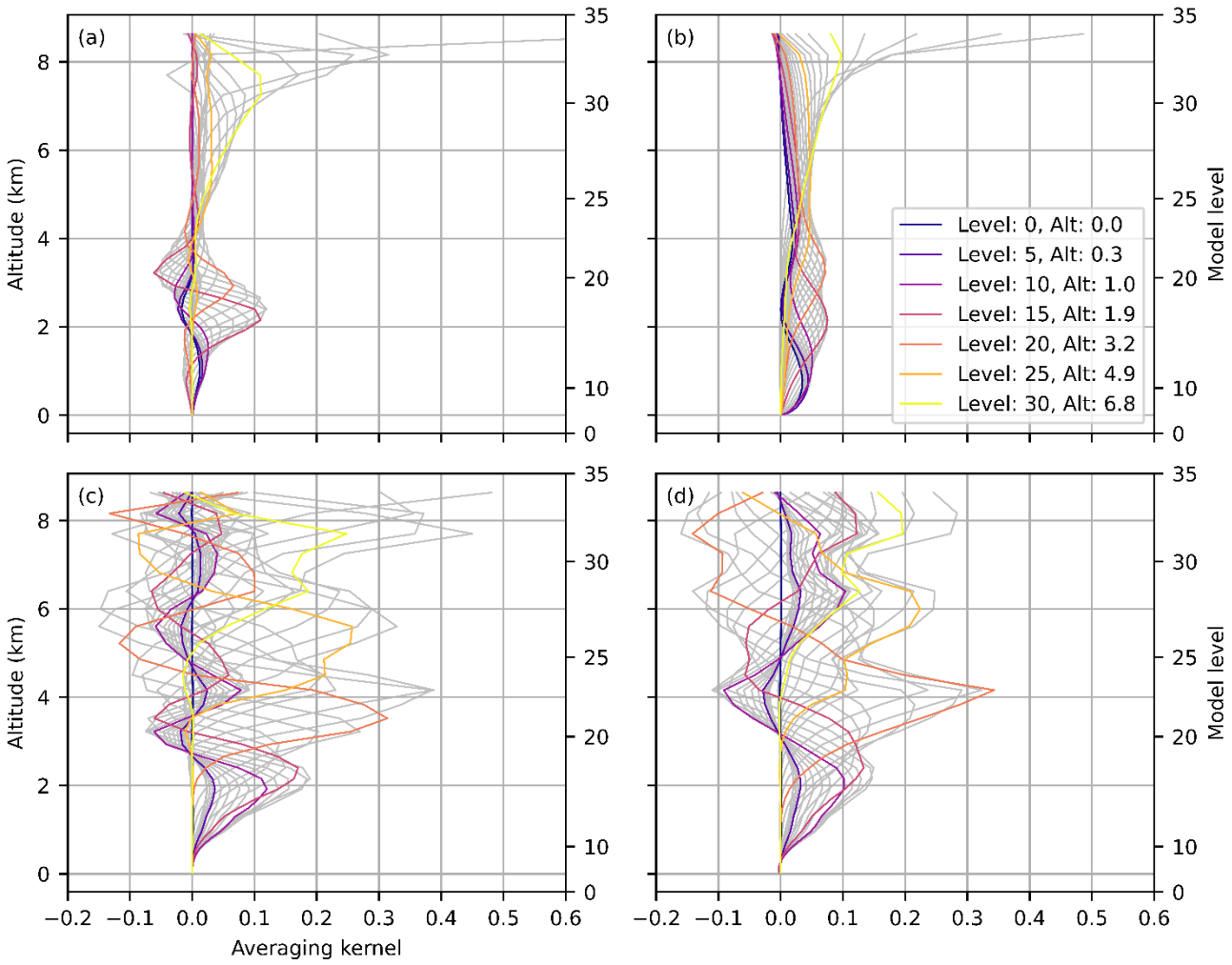

Figure S2. TAFTS (a and c) and ARIES (b and d) averaging kernels for temperature (top row) and water vapour (bottom row). The TAFTS retrieval is the reduced range, full resolution retrieval described in section 4.3. The averaging kernels represent the extent to which the retrieved state is dependent on the true atmospheric state. The TAFTS averaging kernels are generally sharper indicating better vertical resolution particularly for water vapour (c). For temperature the averaging kernels for both instruments are generally low other than at the level closest to the aircraft.

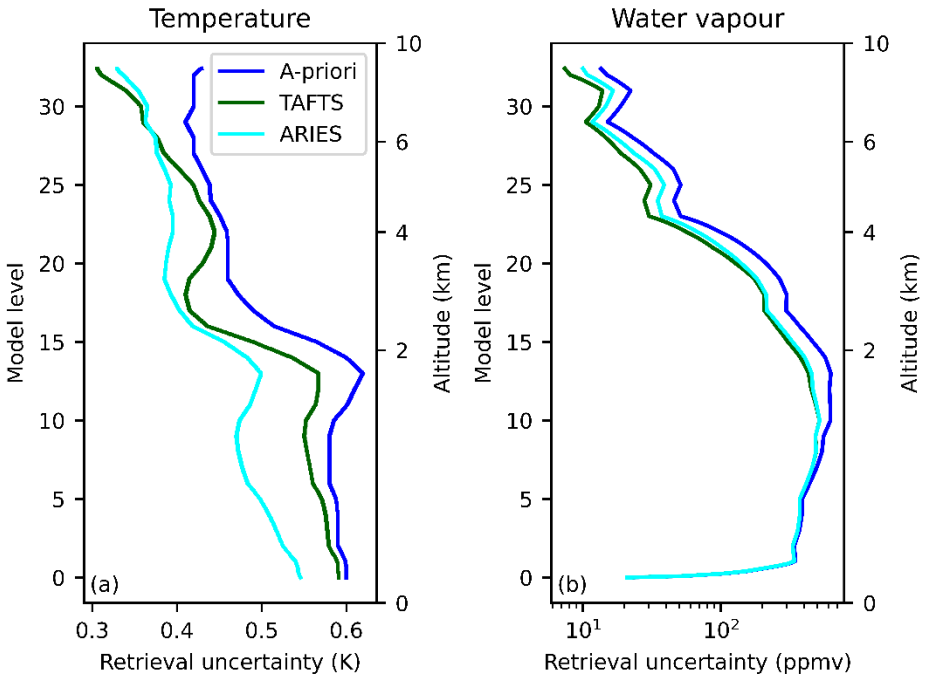

Figure S3. Comparison of standard deviation for (a) temperature and (b) water vapour profiles for the a-priori and TAFTS and ARIES retrievals. The TAFTS retrieval is the reduced range, full resolution retrieval described in section 4.3. The ARIES temperature retrieval has lower standard deviation below model level 27 or 6 km. The TAFTS water vapour retrieval has a lower standard deviation throughout the profile.

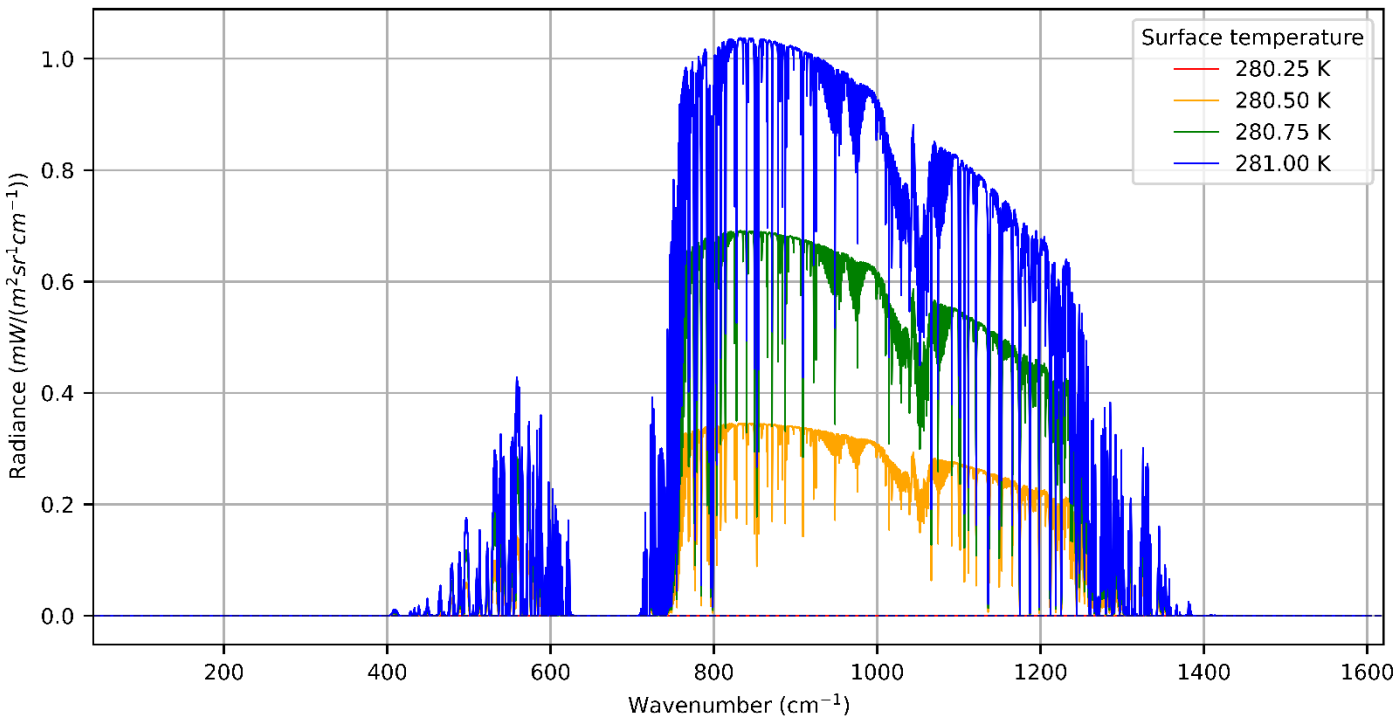

Figure S4. Radiance differences between the dropsonde simulation and simulations with increased surface temperature (see Text S2).

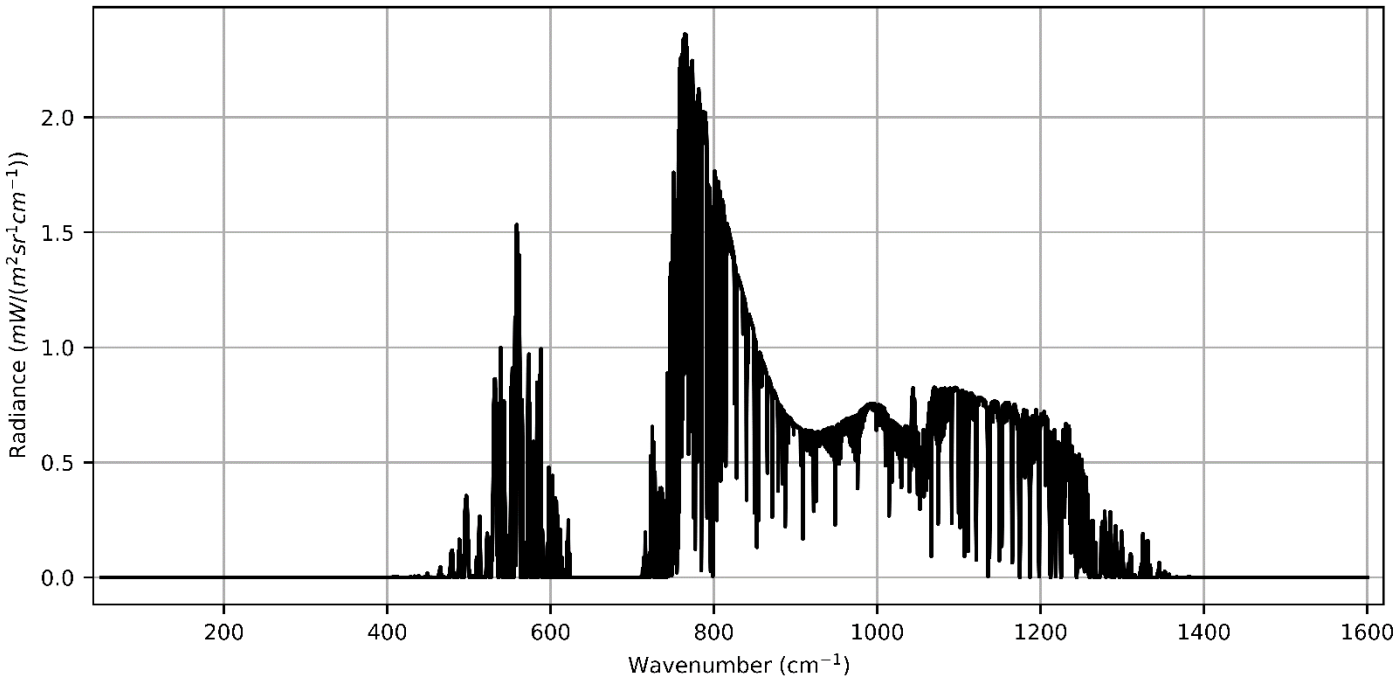

Figure S5. Radiance differences between the standard dropsonde simulation and an equivalent simulation using blackbody surface emissivity (see Text S2).

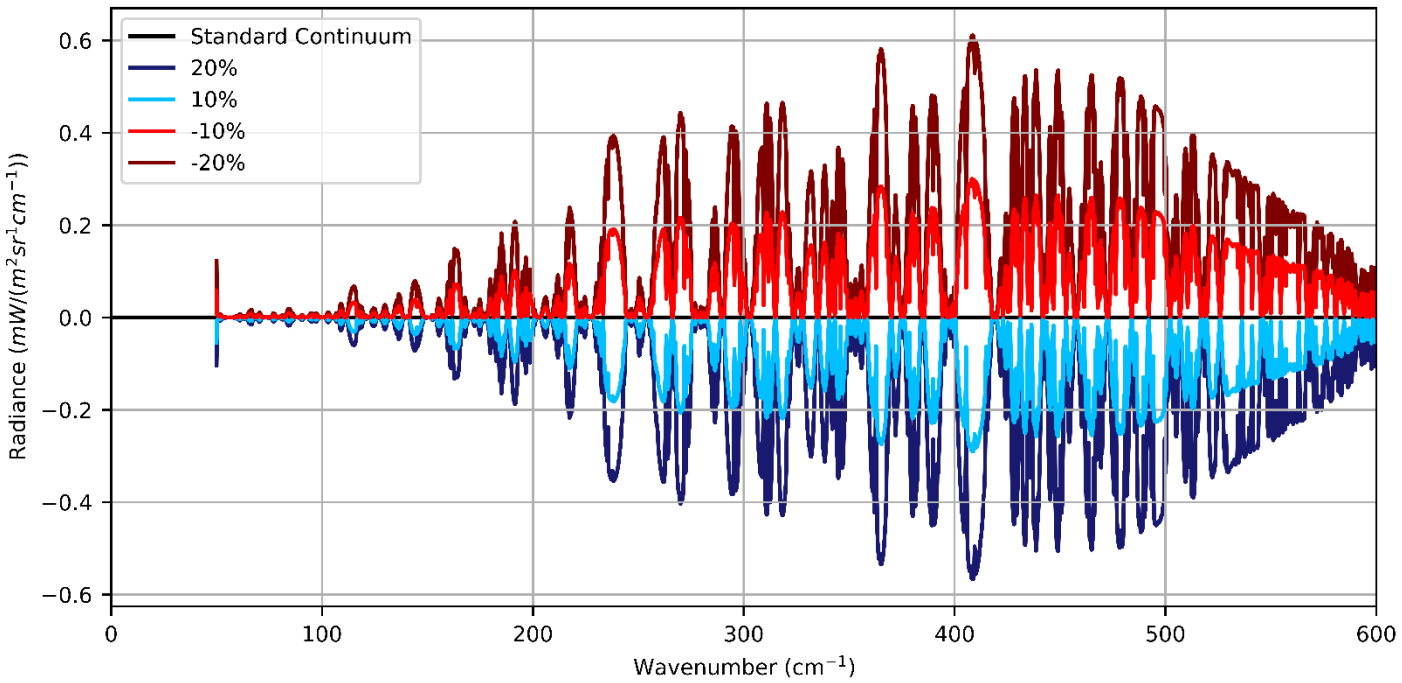

Figure S6. Radiance differences between simulations of the dropsonde case using the best estimate of the water vapour continuum and perturbed versions of the water vapour continuum (see Text S2).

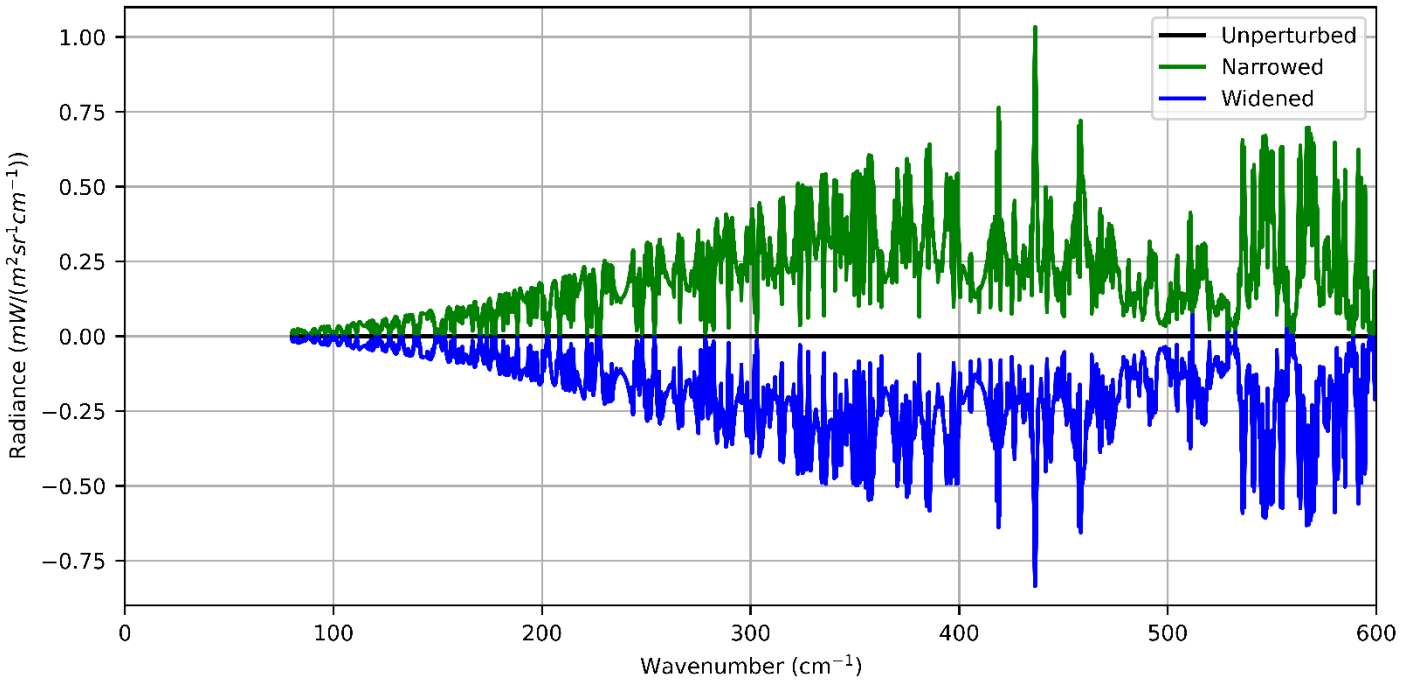

Figure S7. Radiance differences between simulations of the dropsonde case using the best estimate of the water vapour line strengths and perturbed versions of the water vapour line strengths (see Text S2).